ADVANCED MATERIALS
www.advmat.de

High-Voltage Aqueous Na-Ion Battery Enabled by Inert-Cation-Assisted Water-in-Salt Electrolyte

Liwei Jiang, Lilu Liu, Jinming Yue, Qiangqiang Zhang, Anxing Zhou, Oleg Borodin, Liumin Suo,* Hong Li, Liquan Chen, Kang Xu, and Yong-Sheng Hu**

Water-in-salt (WiS) electrolytes provide a new pathway to widen the electrochemical window of aqueous electrolytes. However, their formulation strongly depends on the solubility of the chosen salts, imposing a stringent restriction on the number of possible WiS systems. This issue becomes more severe for aqueous Na-ion batteries (ANIBs) owing to the relatively lower solubility of sodium salts compared to its alkaline cousins (Li, K, and Cs). A new class of the inert-cation-assisted WiS (IC-WiS) electrolytes containing the tetraethylammonium (TEA^+) inert cation is reported. The Na IC-WiS electrolyte at a superhigh concentration of 31 mol kg^{-1} exhibits a wide electrochemical window of 3.3 V, suppresses transition metal dissolution from the cathode, and ensures singular intercalation of Na into both cathode and anode electrodes during cycling, which is often problematic in mixed alkali cation systems such as K–Na and Li–Na. Owing to these unique advantages of the IC-WiS electrolyte, the $NaTiOPO_4$ anode and Prussian blue analog $Na_{1.88}Mn[Fe(CN)_6]_{0.97}\cdot 1.35H_2O$ cathode can be coupled to construct a full ANIB, delivering an average voltage of 1.74 V and a high energy density of 71 Wh kg^{-1} with a capacity retention of 90% after 200 cycles at 0.25C and of 76% over 800 cycles at 1C.

Large-scale energy storage technologies are indispensable for the integration of intermittent renewable energy sources such as wind and solar power into the grid.[1,2] Among various energy storage technologies, aqueous rechargeable metal ion batteries represent promising candidates for large-scale energy storage owing to their inherent safety, nontoxicity, and low cost.[3] However, compared with commercial nonaqueous batteries, aqueous batteries suffer from numerous drawbacks stemming from the aqueous electrolyte usage. On the one hand, the output voltage and energy density are limited by the inherently narrow electrochemical window of the aqueous electrolyte (1.23 V under thermodynamic conditions). On the other hand, the Coulombic efficiency and cycling stability are poor due to significant evolution of hydrogen and oxygen, especially at low rates (below 0.5C).[3–5]

Recently, water-in-salt (WiS) electrolytes expanded the electrochemical window into 3 V regime and have supported Li-ion chemistries above 2 V to deliver high energy density and excellent cycling stability owing to the solid electrolyte interphase (SEI) formation on anode surfaces.[6] This concept was successfully transferred to other types of aqueous electrochemical energy storage devices, including Na/K/Mg/Zn-ion batteries[7–15] and supercapacitors.[16,17] One of the remaining challenges in these attempts is the development of a suitable sodium WiS electrolyte, because the existing sodium electrolytes are still far away from meeting all the requirements simultaneously, including a high salt solubility, a source for SEI chemistry (fluorine-containing salt), and a high chemical and electrochemical stability in aqueous environment. At room temperature, the solubility of typical sodium salts with fluorinated anions, such as sodium triflate (NaOTF) and sodium (bis(trifluoromethane sulfonyl)-imide) (NaTFSI), is less than half (9–10 mol kg^{-1})[7] as their Li or K counterparts (20–22 mol kg^{-1}),[6,12] hence the sodium WiS electrolytes based on NaOTF and NaTFSI salts are unable to fully realize the advantages of superconcentrated electrolytes. In the Li-based WiS electrolytes, utilization of Li bisalt mixtures significantly increased salt concentration up to 28 mol kg^{-1}: LiTFSI-LiOTF (21 mol kg^{-1} LiTFSI + 7 mol kg^{-1} LiOTF)[8] and LiOTF-LiBETI (lithium bis(pentafluoroethanesulfonyl)imide) (19.4 mol kg^{-1} LiOTF + 8.3 mol kg^{-1} LiBETI).[13] This approach,

L. Jiang, Dr. L. Liu, J. Yue, Q. Zhang, A. Zhou, Prof. L. Suo, Prof. H. Li, Prof. L. Chen, Prof. Y.-S. Hu
Key Laboratory for Renewable Energy
Beijing Key Laboratory for New Energy Materials and Devices
Beijing National Laboratory for Condensed Matter Physics
Institute of Physics
Chinese Academy of Sciences
Beijing 100190, China
E-mail: suoliumin@iphy.ac.cn; yshu@iphy.ac.cn

L. Jiang, Dr. L. Liu, J. Yue, Q. Zhang, A. Zhou, Prof. L. Suo, Prof. Y.-S. Hu
Center of Materials Science and Optoelectronics Engineering
University of Chinese Academy of Sciences
Beijing 100049, China

Dr. O. Borodin, Dr. K. Xu
Electrochemistry Branch
Sensor and Electron Devices Directorate
Combat Capabilities Development Command U.S. Army Research Laboratory
Adelphi, MD 20783, USA
E-mail: oleg.a.borodin.civ@mail.mil

Prof. L. Suo, Prof. H. Li, Prof. Y.-S. Hu
Yangtze River Delta Physics Research Center Co. Ltd
Liyang 213300, China

The ORCID identification number(s) for the author(s) of this article can be found under https://doi.org/10.1002/adma.201904427.

DOI: 10.1002/adma.201904427

however, is less fruitful for the Na salts, where solubility of the Na bisalt mixtures is only slightly higher than that of Na single salt, for example, NaOTF-NaTFSI (9 mol kg^{-1} NaOTF + 2 mol kg^{-1} NaTFSI) versus NaOTF (9.3 mol kg^{-1}). It is possible to form a higher concentration electrolyte by mixed-cation bisalt mixtures such as NaOTF-KOTF (9 mol kg^{-1} NaOTF + 8 mol kg^{-1} KOTF, 22 mol kg^{-1} KOTF + 4 mol kg^{-1} NaOTF) electrolyte tested in this work. However, the presence of other cations might result in the mixed-cation cointercalation to electrodes, which has a severe negative impact on battery performance including continuous voltage evolution during cycling process.[18,19]

To address the above issues, we propose a new class of inert-cation assisted water-in-salt (IC-WiS) electrolytes containing tetraethylammonium triflate (TEAOTF) salt. The Na IC-WiS electrolyte (NaOTF-TEAOTF) realizes a superhigh total concentration of 31 mol kg^{-1} (9 mol kg^{-1} NaOTF + 22 mol kg^{-1} TEAOTF), thus expanding the electrochemical stability window to 3.3 V. Moreover, this approach avoids the mixed-cation cointercalation phenomenon during cycling because the radius of the TEA^+ cation is so large that it cannot be intercalated into most of electrodes, even into the Prussian blue analogue (PBA) with an open framework structure. Here, $NaTiOPO_4$ with a low redox potential of 1.5 V (vs Na^+/Na) is successfully utilized as an anode in aqueous electrolyte and is coupled with PBA $Na_{1.88}Mn[Fe(CN)_6]_{0.97}\cdot 1.35H_2O$ cathode. Moreover, the Na IC-WiS electrolyte effectively suppresses the dissolution of transition metal (Fe and Mn) from the $Na_{1.88}Mn[Fe(CN)_6]_{0.97}\cdot 1.35H_2O$ cathode, therefore remarkably improving battery cycling performance. Furthermore, the $Na_{1.88}Mn[Fe(CN)_6]_{0.97}\cdot 1.35H_2O$// Na IC-WiS//$NaTiOPO_4$ full battery, with a high energy density of 71 Wh kg^{-1}, exhibits outstanding cycling stability at both low and high rates, thanks to unique combination of the Na IC-WiS electrolyte properties, whose physicochemical properties are systematically studied by advanced experimental techniques together with molecular scale modeling and simulations.

Salt-in-water (SiW) and WiS electrolytes are defined as aqueous solutions in which the weight and volume ratios of the dissolved salt to water are below 1 and above 1, respectively.[6] **Figure 1**a displays the total salt solubility versus the weight ratio of salt to water for kind of Na salt systems (detailed data listed in Table S1 in the Supporting Information), which clearly indicates the direction of from SiW to WiS electrolytes. Note that the data of sodium bis(trifluoromethylsulfonyl)imide (NaFSI) aqueous solution is excluded, because it shows severe water hydrolysis in the aqueous solution especially at elevated temperatures, leading to a reduced PH value of the electrolyte.[20]

The saturated solutions of commonly used salts (2 mol kg^{-1} Na_2SO_4, 6 mol kg^{-1} NaCl, 4.5 mol kg^{-1} NaOAc, and 10 mol kg^{-1} $NaNO_3$) belong to SiW electrolytes owing to a salt/water weight ratio below 1. The 9.3 mol kg^{-1} NaOTF, 9 mol kg^{-1} NaTFSI, and 17 mol kg^{-1} $NaClO_4$ solutions are identified as WiS electrolytes due to a salt/water weight ratio above 1, which possess the advantages similar to the Li-based WiS electrolytes.[6] However, they are not good enough for high-voltage ANIBs. Specifically, both the NaOTF- and NaTFSI-based WiS electrolytes can form a favorable SEI containing fluorine on anode surfaces,[7] but the formed SEI might not be stable enough as does their Li-based counterparts due to a lower concentration compared with LiOTF- and LiTFSI-based WiS electrolytes (≈9 mol kg^{-1} vs ≈22 mol kg^{-1}).[21] The $NaClO_4$-based WiS electrolyte possesses a higher concentration of 17 mol kg^{-1}, but it does not form a favorable SEI containing fluorine during cycling due to the absence of fluorine in anions. Therefore, the aqueous batteries assembled by 17 mol kg^{-1} $NaClO_4$ electrolyte usually exhibit a poor cycling stability at low current density,[10,22] although a SEI containing Na_2CO_3 may exist on anode surfaces.[23]

To further increase the salt proportion in aqueous solutions, mixed-anion and mixed-cation salt electrolytes have been explored as shown in Figure 1a, demonstrating that the mixed alkali cation (Na–K and Na–Li) solutions can achieve higher salt concentration compared to the mixed anion (OTF-TFSI, OTF-ClO_4, and TFSI-ClO_4) solutions. However, the presence of other alkali cations such as K^+ or Li^+ is likely to induce an undesirable cation cointercalation into the Na-based electrodes.

In this work, we introduced a salt with a large radius organic cation such as tetraethylammonium (TEA^+) in the 9 mol kg^{-1} NaOTF electrolyte (namely the Na IC-WiS electrolyte) to minimize the negative effects associated with the possible cointercalation of other alkali cations to the Na-based electrodes. Impressively, the proposed Na IC-WiS electrolyte with a formula of $Na_{0.29}TEA_{0.71}OTF\cdot 1.79H_2O$ (Table S1, Supporting Information) shows the highest total salt concentration of 31 mol kg^{-1} (9 mol kg^{-1} NaOTF + 22 mol kg^{-1} TEAOTF), corresponding to the highest salt/water weight ratio of 7.69 as shown in Figure 1a. It provides wider electrochemical window than that of 9 mol kg^{-1} NaOTF electrolyte on various current collectors (Figure 1b; Figure S1a,b, Supporting Information). The overall electrochemical stability window of Na IC-WiS electrolyte is significantly expanded from 2.7 to 3.3 V when using Al and Ti meshes as the negative and positive current collectors, respectively. The insets of Figure 1b illustrate the multiple advantages of the Na IC-WiS electrolyte, such as the wide electrochemical window, the low viscosity, the SEI containing NaF on the anode, mitigating dissolution of the electrodes and the inertness of the large radius TEA^+ cation to electrodes.

It is worth noting that the Na IC-WiS electrolyte can also be transplanted to other aqueous metal ion (Li, K, Zn, and Al) systems. As listed in Table S2 (Supporting Information), these corresponding IC-WiS electrolytes with Li, K, Zn, and Al salts can also achieve high enough total concentration, which would represent promising candidates for developing high-voltage aqueous batteries.

The maximum solubility of the TEAOTF salt in the 9 mol kg^{-1} NaOTF electrolyte is about 21–22 mol kg^{-1} (Figure S2, Supporting Information) at 25 °C according to the differential scanning calorimetry (DSC) results, and the 9 mol kg^{-1} NaOTF +22 mol kg^{-1} TEAOTF electrolyte can stably exist in liquid state at 25 °C. Despite high overall salt concentration of 31 mol kg^{-1}, its viscosity is only 30.2 mPa s at 25 °C (**Figure 2**a; Figure S3, Supporting Information), which is nearly one order of magnitude lower than previous reported values[13,24] for the Li-based bisalt electrolytes (203 mPa s at 30 °C and 374 mPa s at 25 °C for 19.4 mol kg^{-1} LiOTF + 8.3 mol kg^{-1} LiBETI and 8 mol kg^{-1} LiOAc + 32 mol kg^{-1} KOAc electrolytes, respectively). Benefited from the low viscosity, the ionic conductivity of the 9 mol kg^{-1} NaOTF + 22 mol kg^{-1} TEAOTF electrolyte (11.2 mS cm^{-1}) is much higher than those of the 19.4 mol kg^{-1} LiOTF + 8.3 mol kg^{-1} LiBETI and 8 mol kg^{-1} LiOAc + 32 mol kg^{-1} KOAc electrolytes (3 and 5.3 mS cm^{-1}, respectively).

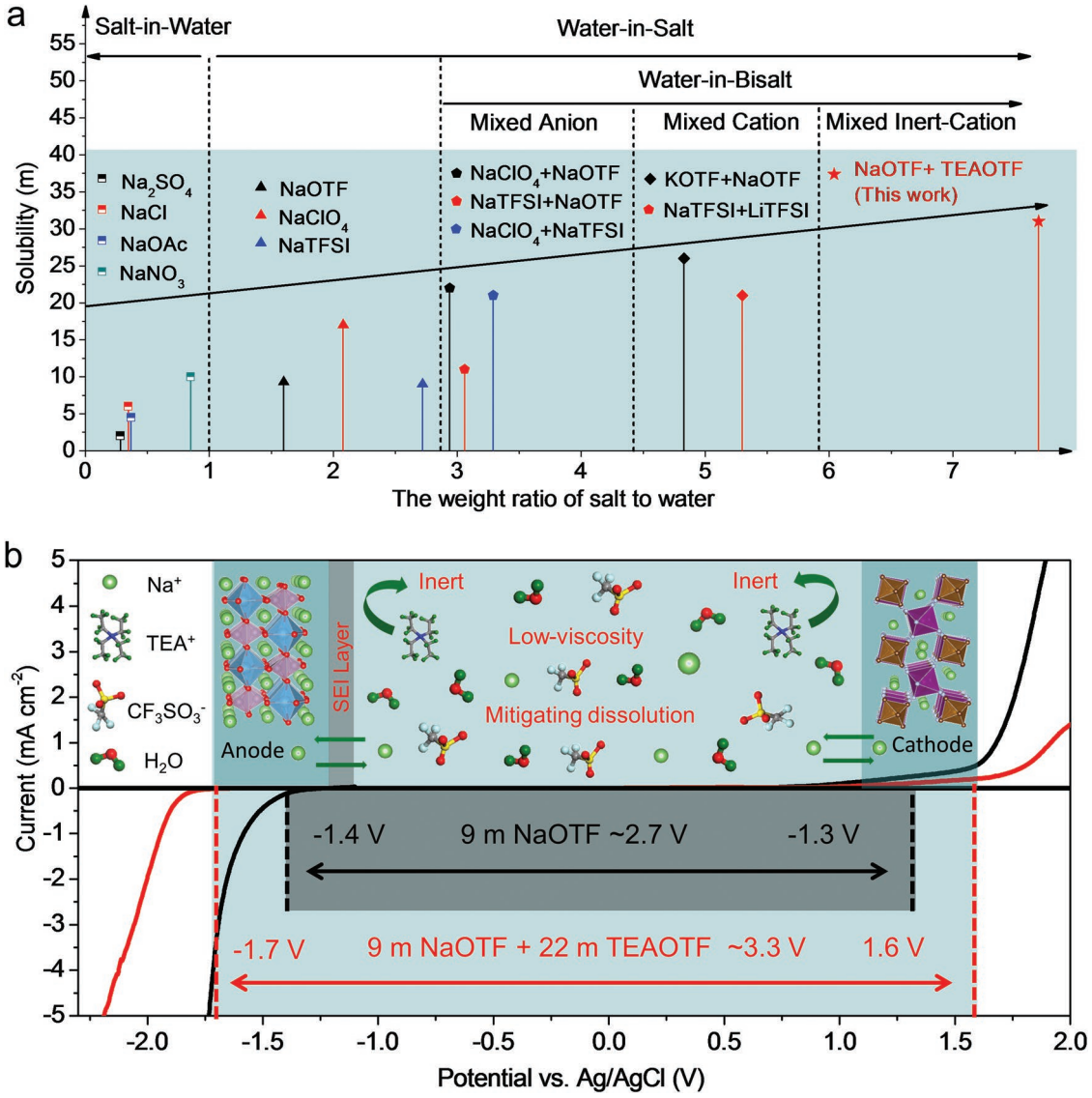

Figure 1. The Na inert-cation-assisted water-in-salt (IC-WiS) electrolyte. a) The solubility of salts versus the weight ratio of salt to water. b) The electrochemical voltage window of 9 mol kg^{-1} NaOTF electrolyte and Na IC-WiS electrolyte (9 mol kg^{-1} NaOTF +22 mol kg^{-1} TEAOTF) from the linear sweep voltammetry measurements performed in the three-electrode cell at the scanning rate of 10 mV s^{-1}. The Al and Ti meshs are chosen as the negative and positive electrode current collectors, respectively. The insets illustrate major advantages of the Na IC-WiS electrolyte for the aqueous Na-ion batteries, including the wide electrochemical window, the low viscosity, the favorable SEI containing NaF on the anode surface, mitigating dissolution of the electrodes and the inertness of TEA^+ cation intercalation to electrodes.

Note that the viscosity of 9 mol kg^{-1} NaOTF + 8 mol kg^{-1} TEAOTF electrolyte (13.7 mPa s) at 25 °C is lower than that of 9 mol kg^{-1} NaOTF + 8 mol kg^{-1} KOTF electrolyte (16.5 mPa s) (Table S3, Supporting Information), which indicates that the favorable transport properties of Na IC-WiS electrolyte are clearly related to the unique physicochemical feature of the TEAOTF salt. The relationship of concentration and the ionic conductivity for XOTF (X = Li, Na, K, and TEA) aqueous solutions are shown in Figure 2b (detailed data listed in Table S4, Supporting Information). Typically, the ionic conductivity of a liquid solution can be classified as concentration-controlled region (C-region) in dilute regime and mobility-controlled region (M-region) in concentrated regime.[25] In the C-region, ionic conductivity increases with increasing concentration of charge carriers for XOTF (X = Li, Na, and K) electrolytes, while in the M-region, further salt concentration increase leads to the conductivity drop owing to the ion pair and aggregate formation and increased viscosity.[25] In contrast, the ionic conductivity of the TEAOTF salt solutions experiences little change in both regions, indicating that the TEAOTF salt solution possesses different interactions for the cation–anion and salt–water.

To understand the underlying transport features, cation–anion interactions and solvation structure in the Na IC-WiS electrolyte, we performed Raman, nuclear magnetic resonance (NMR) measurements and molecular dynamics (MD) simulations. The MD simulations predict that Na IC-WiS electrolyte

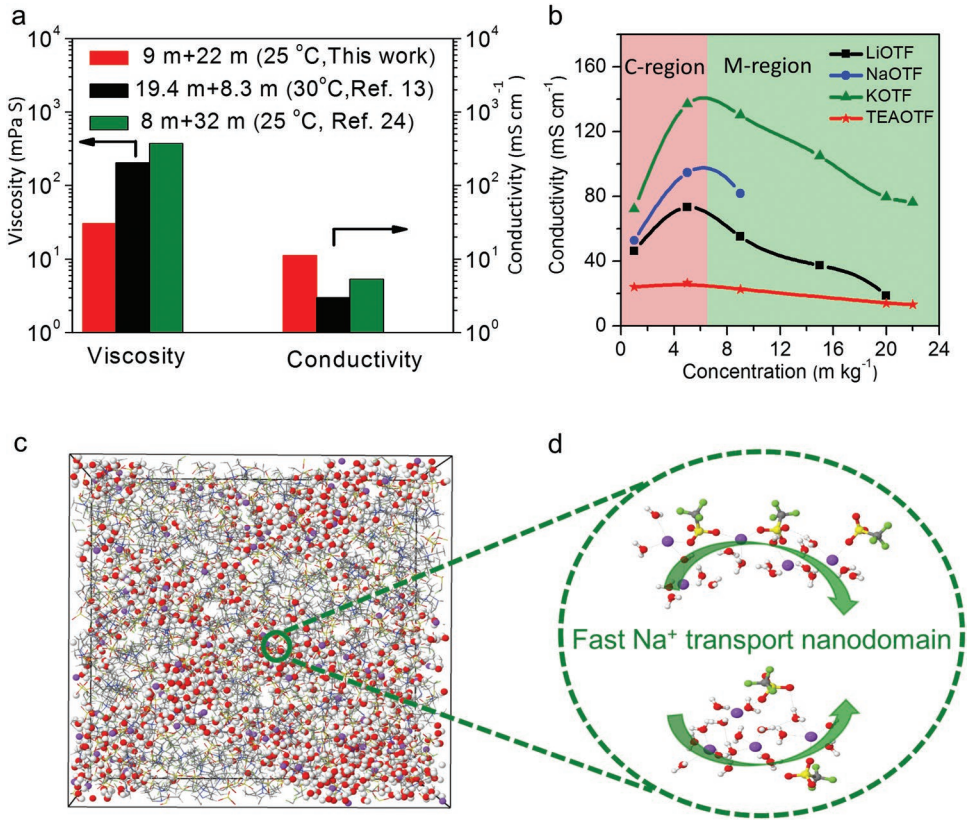

Figure 2. Transport properties of the Na IC-WiS electrolyte. a) The comparison of viscosity and ionic conductivity for 9 mol kg^{-1} NaOTF + 22 mol kg^{-1} TEAOTF, 19.4 mol kg^{-1} LiOTF + 8.3 mol kg^{-1} LiBETI and 8 mol kg^{-1} LiOAc + 32 mol kg^{-1} KOAc electrolytes. b) The concentration dependence of ionic conductivity at 25 °C for LiOTF, NaOTF, KOTF, and TEAOTF aqueous solutions, respectively. c) A snapshot of the MD simulation box for the Na IC-WiS electrolyte with water and Na^+ highlighted and TEAOTF shown as wireframe. d) The $Na(H_2O)_n$ nanochannels with fast Na^+ transport, extracted from the MD simulations.

has a conductivity of 8.8–9.7 mS cm^{-1} and a viscosity of 28.3–29 mPa s at 303 K (Table S5, Supporting Information), which are in good agreement with experimental values, demonstrating that the quantum chemistry-based polarizable force field (APPLE&P) can accurately capture the ion-ion and ion-solvent interactions. Analyses of the ion and water diffusion coefficients (Table S5, Supporting Information) reveal that the Na^+ cation diffusion is the second fastest after water, followed by the OTF^- anions and TEA^+ cations in Na IC-WiS electrolyte. Despite a high TEAOTF salt content (71% molar ratio) in the Na IC-WiS electrolyte, the apparent transference number of Na^+ remains about 0.23 at 303 K, which is close to the 0.29 of TEA^+ as listed in Table S5 (Supporting Information). The value of 0.23 is comparable with those (0.23–0.3) of some Na-based gel polymer electrolytes[26,27] and slightly lower than that (0.4) of Li-based electrolyte,[28] which indicates that the Na IC-WiS electrolyte should possess an acceptable concentration overpotential during cycling.

A snapshot of the MD simulation box (Figure 2c) shows that the electrolyte structure is not uniform on the nanoscale and is independent of the initial simulation conditions (Figure S4, Supporting Information). A network of the interpenetrating transient $Na^+(H_2O)_n$ nanodomains with fast Na^+ transport pathway (Figure 2d) forms within the TEAOTF framework. The Na^+ cations are strongly partitioned to these $Na^+(H_2O)_n$ nanodomains and away from the TEAOTF. Thus the Na^+ transport mechanism in the Na IC-WiS electrolyte is closer to the Na^+ and Li^+ transport in aqueous WiS electrolytes[29,30] and is different from the Na^+ transport in room temperature ionic liquids (RTILs) where a motion of the $Na(TFSI)_n$ clusters and the Na-TFSI exchange were observed.[31] Analysis of the radial distribution functions (RDFs) (Figure S5, Supporting Information) confirms that the Na^+ cations have higher affinity to water than to the OTF^- anions and indicates an unexpectedly low magnitude of the first Na-O(TFSI) peak, suggesting significant dissociation of the NaOTF salt dissociation despite overall high salt concentration.

The solvation shell analysis confirms that 55% of Na^+ exist as free cations (not coordinated by OTF^-) and mostly diffuse together with water, while the other Na^+ participate in the contact ion pair (CIP = 32%) and aggregate pair (AGG = 13%) formation by binding to both OTF^- anions and water (Figure S6, Supporting Information). The Na^+ solvation shells in the concentrated electrolytes differ from those in the dilute electrolytes,[7] which may affect the way (hydrated or dehydrated) of Na^+ intercalation to electrodes. This issue deserves further study in the future. The Na^+ cations largely move via the vehicular mechanism by diffusing together with their hydration shells,[32] because of the high fraction of free $Na^+(H_2O)_n$ (n = 4, 5) solvates (Figure S6, Supporting Information) and

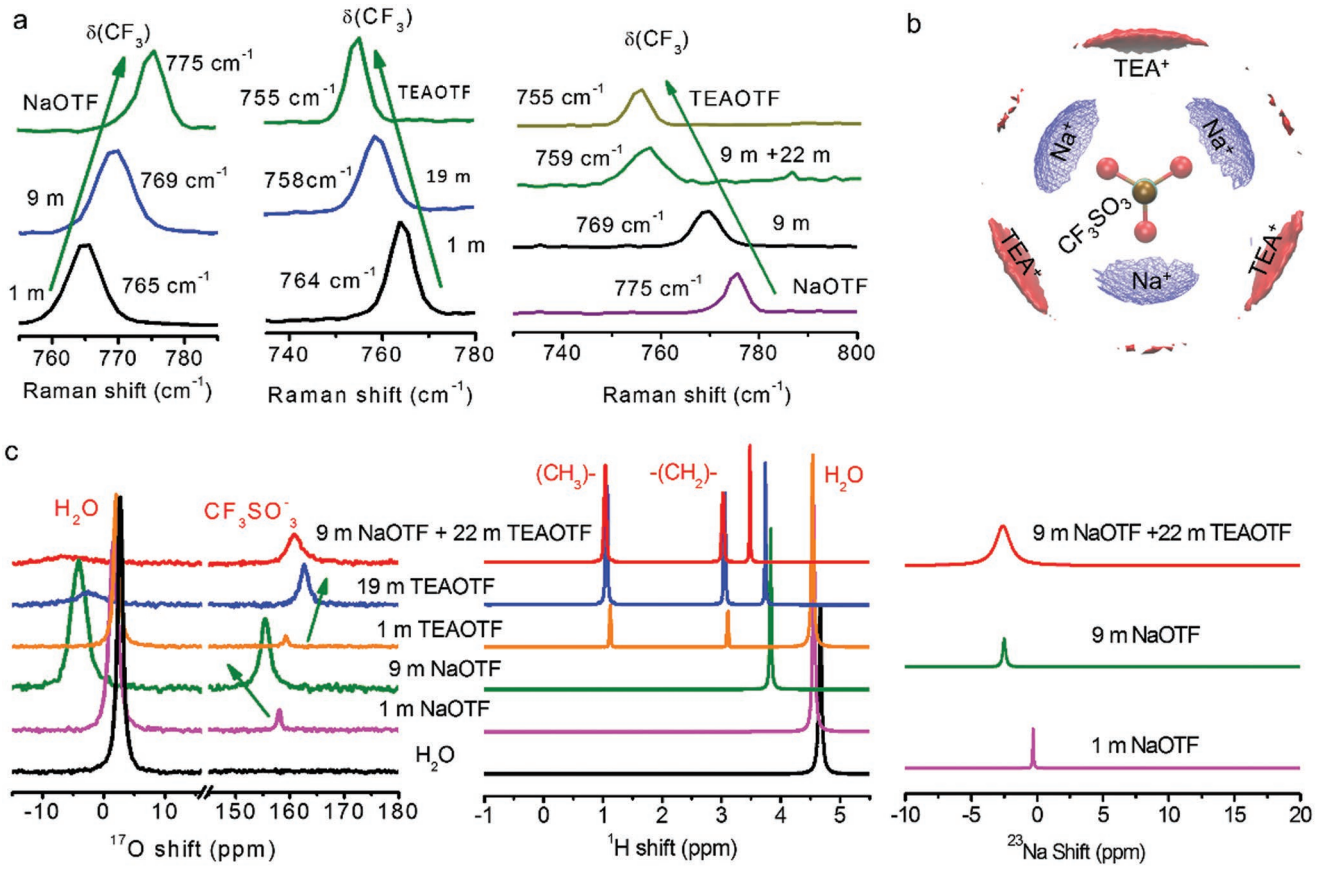

Figure 3. The cation–anion and ion–water interactions in the Na IC-WiS electrolyte solutions. a) The $\delta(CF_3)$ Raman bands for NaOTF powder, NaOTF aqueous solutions (1 and 9 mol kg^{-1}), TEAOTF powder and TEAOTF aqueous solutions (1 and 19 mol kg^{-1}) and 9 mol kg^{-1} NaOTF + 22 mol kg^{-1} TEAOTF electrolyte. b) Isosurface showing most probable positions (8.5 times the average) of the TEA^+ nitrogen atom (red mesh) and Na^+ (blue mesh) around the $CF_3SO_3^-$ anion. Note that the average position of fluorine atoms is shown due to CF_3^- group rotation. c) The ^{17}O, ^1H and ^{23}Na NMR chemical shift in different solutions. The ^{17}O signal of H_2O and $CF_3SO_3^-$, ^1H signal of H_2O, (CH_3)– in TEA^+ and $–(CH_2)$– in TEA^+ are marked in (c).

the long Na–water residence time of 1.5 ns, resulting in the Na^+ motion of 7.9 Å with its hydration shell during one residence time. The Na^+/OTF^- contact ion pairs and aggregates compatibilize the $Na^+(H_2O)_nOTF$ and TEAOTF domains and prevent their phase separation.

The Raman spectra of XOTF (X = Na, TEA) solutions and their solid powders (**Figure 3**a; Figures S7–S9, Supporting Information) demonstrate that the symmetric bending mode, $\delta(CF_3)$,[33,34] exhibits a blueshift (765 cm^{-1} of 1 mol kg^{-1} to 769 cm^{-1} of 9 mol kg^{-1}) as the NaOTF salt concentration increases; in contrast, a redshift (764 cm^{-1} of 1 mol kg^{-1} to 758 cm^{-1} of 19 mol kg^{-1}) occurs in the TEAOTF case. The reversed trend suggests that the degree of cation–anion interaction in solutions follow the order of Na^+-OTF^- > H_3O^+-OTF^- > TEA^+-OTF^-, which can also explain well the trend of the $\delta(CF_3)$ bending modes as shown in Figure 3a: crystal NaOTF (775 cm^{-1}) > 9 mol kg^{-1} NaOTF electrolyte (769 cm^{-1}) > 9 mol kg^{-1} NaOTF+22 mol kg^{-1} TEAOTF electrolyte (759 cm^{-1}) > crystal TEAOTF (755 cm^{-1}). The weaker interaction of TEA^+-OTF^- than that of Na^+-OTF^- is attributed to the larger radius (3.6 Å) of TEA^+ than that of Na^+ (1.02 Å) (Table S6, Supporting Information).[35–37] The relatively weak interaction of the TEA^+ with OTF^- and the hydrated $Na^+(H_2O)_n$ with OTF^- are likely behind the low viscosity of Na IC-WiS electrolyte as the ion–water and cation–anion interactions are known to largely determine the electrolyte viscosity.[38]

The MD simulations revealed that the TEA^+ and Na^+ cations have quite different spatial 3D distribution and coordination motifs with the OTF^- anions (Figure 3b; Figure S10, Supporting Information). The Na^+ cations prefer the monodentate binding to $O(OTF^-)$, leading to a blueshift of the $\delta(CF_3)$ Raman band as ion pairs form in concentrated electrolytes, in agreement with experimental observations (Figure 3a). The TEA^+ cations, on the other hand, prefers to bind in between of the two $O(OTF^-)$ in a bidentate configuration (Figure S11, Supporting Information) resulting in no $\delta(CF_3)$ Raman band shift in aqueous environment. When dielectric constant decreases with increasing TEAOTF salt concentration, a redshift of $\delta(CF_3)$ Raman band is predicted in DFT calculations in agreement with experiments (Figure 3a). A strong dependence of vibrational bands on the cation position was also reported for the $\nu(SO_3)$ band[7]

Note that the ^{17}O chemical shift of OTF^- anion (Figure 3c) also exhibits a similar opposite tendency (green arrows in Figure 3c) as the Raman data. Along with the increase of NaOTF concentration, it shows a redshift (158.1 ppm of 1 mol kg^{-1} to 155.4 ppm of 9 mol kg^{-1}); on the contrary, a blueshift (159.2 ppm of

1 mol kg^{-1} to 162.6 of 19 mol kg^{-1}) happens in the TEAOTF case, which further proves that the electronic density around the ^{17}O of OTF^- and interaction of Na^+-OTF^- in NaOTF solutions is larger than those in TEAOTF solutions.

The ^{17}O and ^1H signals in water and cation signals are used to probe the evolution of water and ion environments with salt concentration. As shown in Figure 3c, the ^{17}O signal in H_2O (between −10 and 10 ppm) moves to lower chemical shifts with the increase of NaOTF and TEAOTF concentrations and shifts down to the lowest value of −8.5 ppm in the 9 mol kg^{-1} NaOTF+22 mol kg^{-1} TEAOTF electrolyte. Similarly, the ^1H signal in H_2O (between 3.2 and 5 ppm) moves to lower chemical shifts with the increase of NaOTF and TEAOTF concentrations and shifts down to the lowest value of 3.5 ppm in the 9 mol kg^{-1} NaOTF + 22 mol kg^{-1} TEAOTF electrolyte (Figure 3c). The above two results confirm the strongest interaction between salt and water in the Na IC-WiS electrolyte. Moreover, the oxygen nuclei exhibit a great peak broadening in the Na IC-WiS electrolyte, indicating a semi solid-state environment, as the 21 mol kg^{-1} LiTFSI WiS electrolyte.[6]

In addition, both the ^1H signal of TEA^+ (between 1 and 3.5 ppm) in the TEAOTF solutions (Figure 3c) and $^{23}Na^+$ signal in the NaOTF solutions (Figure 3c) exhibit a redshift displacement in their chemical shift along with the rise of salt concentration, demonstrating the formation of new ionic structures such as CIPs or AGGs, which agrees with the MD simulation results (Figure S6, Supporting Information).

Here, the PBA $Na_{1.88}Mn[Fe(CN)_6]_{0.97}\cdot 1.35H_2O$ (NaMnHCF) (Table S7 and Figure S12, Supporting Information), with a monoclinic phase in $P2_1/n$ space group and a cubic morphology (Figure S13a,b and Table S8, Supporting Information), is selected as the cathode. Meanwhile, the $NaTiOPO_4$ possessing a low redox potential of ≈1.5 V (vs Na^+/Na) is chosen as the anode, whose Rietveld refinement X-ray diffraction (XRD) and morphology (Figure S14a,b and Table S9, Supporting Information) is consistent with the reported literature.[39] Both electrodes exhibit superior performance, benefiting from the multiple function of the Na IC-WiS electrolyte, as discussed below.

First, the Na IC-WiS electrolyte is effective in diminishing the transition metal dissolution from NaMnHCF cathode during cycling, thus remarkably improving its electrochemical performance. The NaMnHCF cathode exhibits two voltage plateaus (0.7 V and 1.0 V vs Ag/AgCl) in both 9 mol kg^{-1} NaOTF electrolyte and 9 mol kg^{-1} NaOTF + 22 mol kg^{-1} TEAOTF electrolyte (**Figure 4**a). However, the NaMnHCF electrode experiences a rapid capacity decay from 140 to 84 mAh g^{-1} after 50 cycles in 9 mol kg^{-1} NaOTF electrolyte (Figure 4b; Figure S15a, Supporting Information), while the NaMnHCF electrode in 9 mol kg^{-1} NaOTF + 22 mol kg^{-1} TEAOTF electrolyte displays a superior cycling stability, with negligible capacity loss (from 140 to 137 mAh g^{-1}) and improved average Coulombic efficiency (from 92% to 97%) (Figure 4b; Figure S15b, Supporting Information). In fact, the cycling stability of the NaMnHCF cathode is known to closely be associated to the transition metal dissolution in the electrolyte,[40] which was further confirmed by ICP-AES results (Figure 4c). It can be seen that Fe and Mn dissolution amount in 9 mol kg^{-1} NaOTF + 22 mol kg^{-1} TEAOTF electrolyte are much less than those in 9 mol kg^{-1} NaOTF electrolyte (3 ppm vs 19 ppm for Fe, and 4 ppm vs 6 ppm for Mn). The results of transition metal dissolution can also be visually supported by the color change (pale yellow vs dark blue) of the electrolytes after 50 cycles at 1C in the inset of Figure 4c. The dissolution-inhibiting effect is related to the less free water in 9 mol kg^{-1} NaOTF + 22 mol kg^{-1} TEAOTF electrolyte than that in 9 mol kg^{-1} NaOTF electrolyte, which can be demonstrated by the broadening and reduced Raman peak near 3487 cm^{-1} owing to a semi solid-state environment as shown in Figure S16 (Supporting Information).

Second, the Na IC-WiS electrolyte enables a wide cycling voltage range for the $NaTiOPO_4$ anode owing to an expanded electrochemical stability window compared to the 9 mol kg^{-1} NaOTF electrolyte. As shown in Figure 4a, the hydrogen evolution occurs while the redox potential of $NaTiOPO_4$ anode goes lower than −1.3 V at 0.2C during the Na^+ intercalation process in 9 mol kg^{-1} NaOTF electrolyte. In comparison, the $NaTiOPO_4$ anode in Na IC-WiS electrolyte exhibit more reversible capacity (62 mAh g^{-1} vs 53 mAh g^{-1}) and higher initial Coulombic efficiency (51.6% vs 44.2%) thanks to suppressing hydrogen evolution making the discharge potential reaching into lower potential of −1.45 V at 0.2C. In addition, the $NaTiOPO_4$ anode shows high reversible capacity of 53.6 mAh g^{-1} with the capacity retention of 51% after 128 cycles at high rate of 2C (Figures S17 and S18a, Supporting Information). Note that it exhibits better cycling stability (87% retention after 190 cycles at 0.5C) in the pint-sized pouch full cell of AC//$NaTiOPO_4$ (Figure S18b, Supporting Information) due to avoiding the $NaTiOPO_4$ dissolution (Table S10, Supporting Information) resulting from the extremely excessive electrolyte in three-electrode cell.

Third, the large radius of TEA^+ ions in Na IC-WiS electrolyte can remain inertness to intercalation in both NaMnHCF cathode and $NaTiOPO_4$ anode, thus achieving the absence of cointercalation phenomenon, which would occur for the PBA materials in mixed alkali cation systems (Li–Na or K–Na).[18,41,42] As shown in Figure 4d, the inertness of TEA^+ cations can be confirmed by cyclic voltammetry (CV) results of electrodes in 9 mol kg^{-1} NaOTF + 22 mol kg^{-1} TEAOTF and 22 mol kg^{-1} TEAOTF electrolytes, respectively. Both NaMnHCF cathode and $NaTiOPO_4$ anode exhibit reduction peaks (−0.69 and −1.27 V for $NaTiOPO_4$ anode; 0.57, 0.65, and 0.95 V for NaMnHCF cathode) and oxidation peaks (−1.14 and −0.96 V for $NaTiOPO_4$ anode; 0.66, 0.73, and 1.2 V for NaMnHCF cathode). On the contrary, in the 22 mol kg^{-1} TEAOTF electrolyte, the $NaTiOPO_4$ anode shows no redox peak during the Na^+ discharging process and the NaMnHCF cathode presents oxidation peaks (0.61 and 1.17 V) at first charging process and exhibits no redox peak during the discharging process (Figure 4d). Meanwhile, the inertness of TEA^+ is double confirmed by the negligible reversible capacity of both cathode and anode in the 22 mol kg^{-1} TEAOTF electrolyte (Figure S19, Supporting Information).

The assembled NaMnHCF//Na IC-WiS electrolyte// $NaTiOPO_4$ full battery was cycled between 0.7 and 2.6 V as shown in **Figure 5**a. It delivers two discharge voltage plateaus (2.2 and 1.6 V) and shows a high discharge capacity of 41 mAh g^{-1} (based on the total mass of cathode and anode) at the 4th cycle, corresponding to a high energy density of 71 Wh kg^{-1}. Impressively, the full battery not only exhibits excellent long-term cycling stability with a high capacity retention of 90% after 200 cycles at

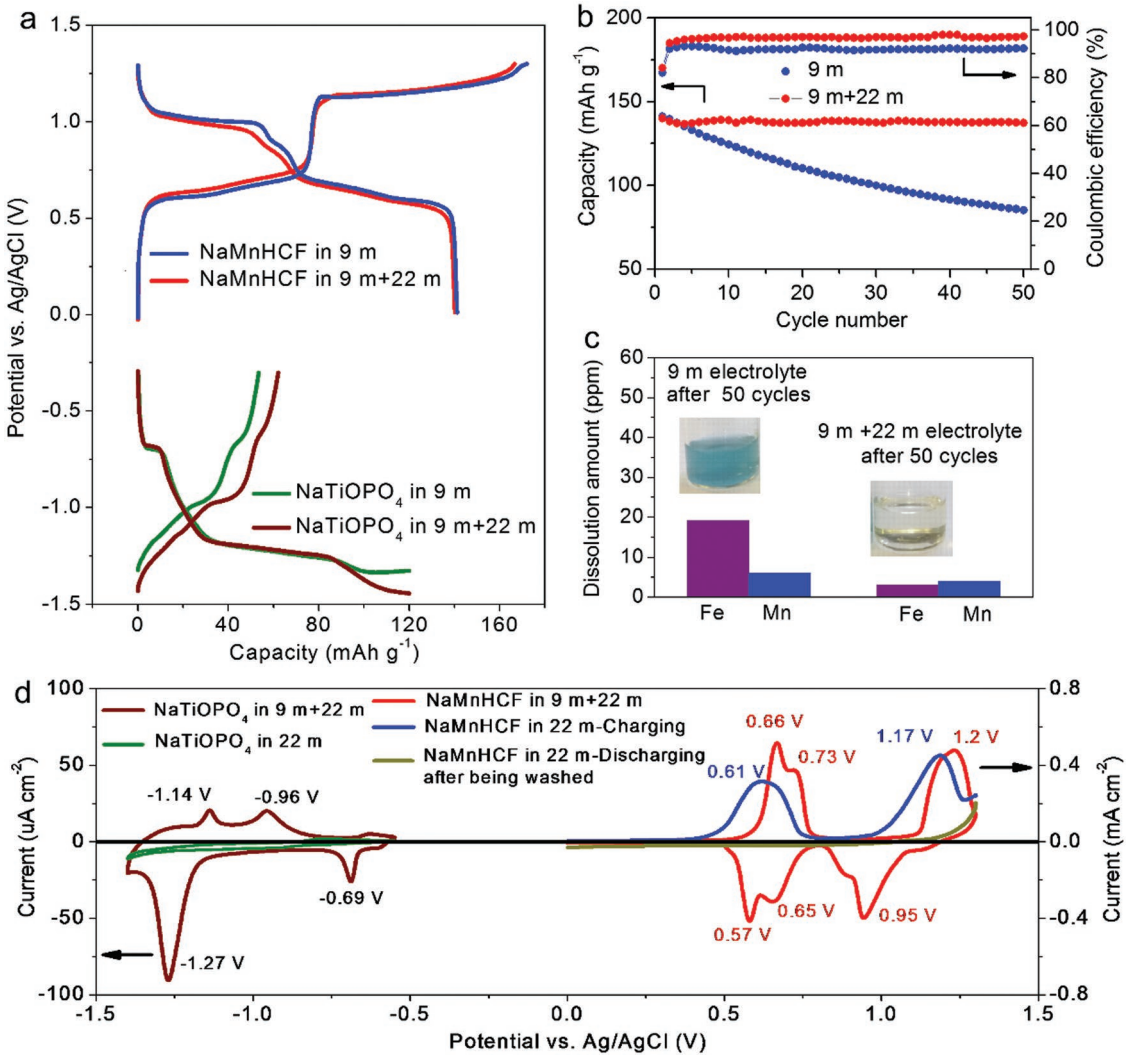

Figure 4. The electrochemical performance of NaMnHCF cathode and $NaTiOPO_4$ anode in 9 $mol\,kg^{-1}$ NaOTF and Na IC-WiS electrolytes. a) First cycle charge–discharge curve of the NaMnHCF cathode at 1C and $NaTiOPO_4$ anode at 0.2C in 9 $mol\,kg^{-1}$ NaOTF and 9 $mol\,kg^{-1}$ NaOTF + 2 2 $mol\,kg^{-1}$ TEAOTF electrolytes, respectively (1C = 0.14 A g^{-1}). b) Discharge capacity and Coulombic efficiency versus cycle number for the NaMnHCF electrode at 1C in the 9 $mol\,kg^{-1}$ NaOTF and 9 $mol\,kg^{-1}$ NaOTF + 22 $mol\,kg^{-1}$ TEAOTF electrolytes, respectively. c) The dissolving amount of the transition metal ions (Fe and Mn) after 50 cycles at 1C in the 9 $mol\,kg^{-1}$ NaOTF and 9 $mol\,kg^{-1}$ NaOTF + 22 $mol\,kg^{-1}$ TEAOTF electrolytes, respectively. The insets show optical photographs of cycled electrolytes. Both electrochemical tests are performed in the three-electrode cell with 4 mL aqueous electrolyte. d) The cyclic voltammetry (CV) profiles of $NaTiOPO_4$ anode and NaMnHCF cathode at 1 mV s^{-1} in 22 $mol\,kg^{-1}$ TEAOTF and 9 $mol\,kg^{-1}$ NaOTF + 22 $mol\,kg^{-1}$ TEAOTF electrolytes, respectively. Note that the NaMnHCF cathode was washed by fresh 22 $mol\,kg^{-1}$ TEAOTF electrolyte after the first charge process.

the low rate of 0.25 C (Figure 5b), but also displays limited self-discharge behavior (inset of Figure 5b). It experiences a small voltage decay initially and then maintains the voltage of ≈2.1 V during a storage duration of 100 h. It also exhibits long-term cycling stability with high capacity retention of 76% after 800 cycles (Figure 5c), which is much better than that (50% retention after 50 cycles at 2C) of the full battery in the 9 $mol\,kg^{-1}$ NaOTF electrolyte (Figure S20a,b, Supporting Information). Moreover, the full cell displays good rate capability (Figure S21a, Supporting Information), with a capacity retention of 78% and 60% at 5C and 10C, respectively, which surpasses some of batteries based on other highly concentrated electrolytes[6,24] (Figure S21b, Supporting Information). The superior performance is attributed to several reasons including a thick (≈10 nm) SEI layer containing NaF on the anode (Figure S22a,b, Supporting Information), stability of electrolyte (Raman spectra in Figure S23 in the Supporting Information), and structural stability of both NaMnHCF cathode (Figures S24a,b and S25a–d, Supporting Information) and $NaTiOPO_4$ (Figures S24c,d and S25e–h, Supporting Information) anode during cycling.

Figure 5d summarizes the average voltage, energy density, and lifespan for this work and other reported ANIB systems[7,10,23,43–48] (the detailed data listed in Table S11 in the Supporting Information), indicating that the NaMnHCF//Na IC-WiS electrolyte//$NaTiOPO_4$ full battery not only exhibits the highest average voltage (1.74 V) and energy density value (71 Wh kg^{-1}), but also achieves a superior long-term cycling life (>800 cycles) with a low capacity loss of 0.03% per cycle.

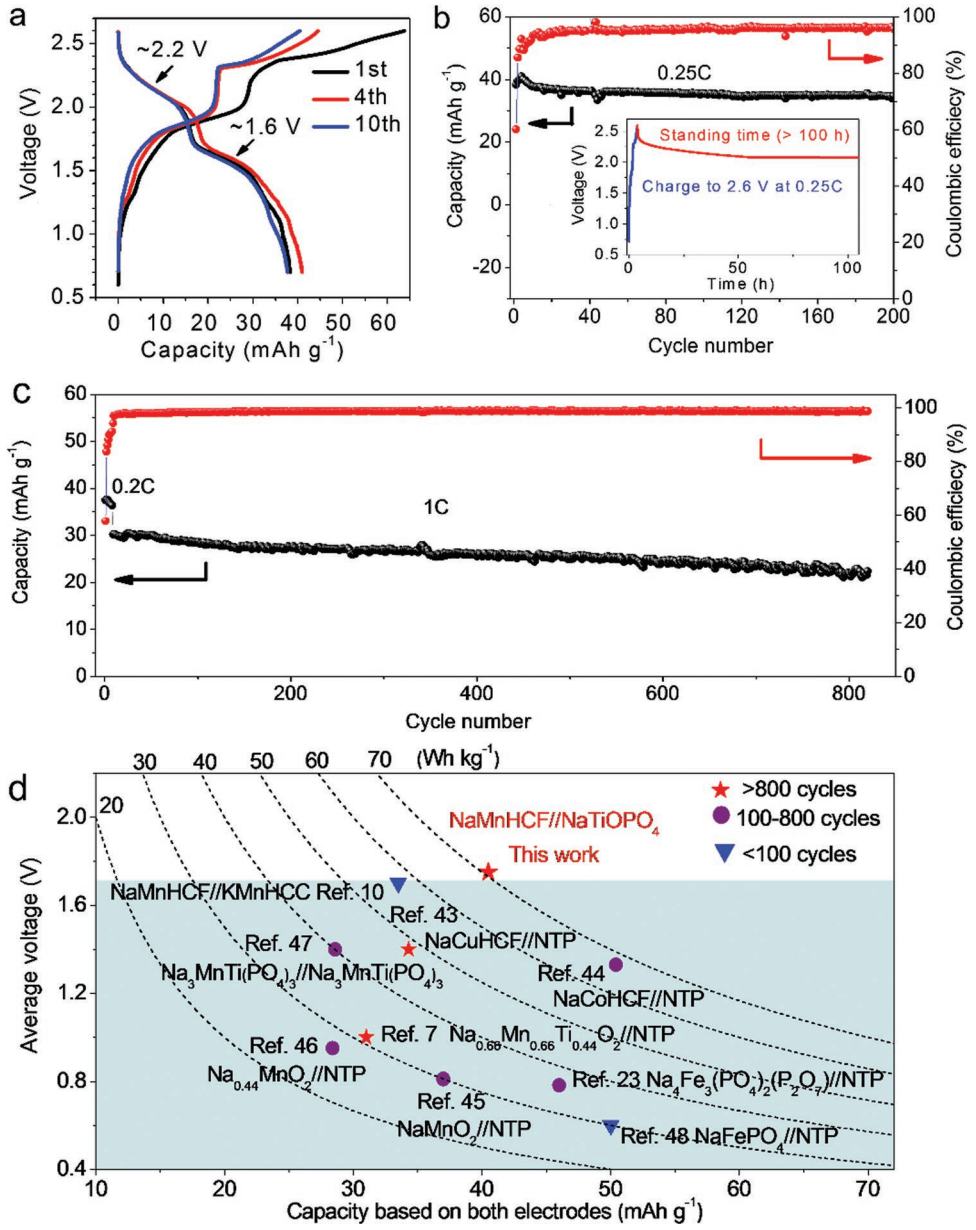

Figure 5. The electrochemical performance of NaMnHCF//$NaTiOPO_4$ full battery. a) The 1st, 4th, and 10th charge–discharge curves of full battery from 0.7 to 2.6 V at 0.25C (1C = 0.14 A g^{-1}). The inset arrows point out the two voltage plateaus (2.2 and 1.6 V) during discharging process. b) The long-term cycling performance of the full battery at 0.25C (1C = 0.14 A g^{-1}). The inset displays the self-discharge performance of the full cell after 17 cycles at 0.25C from 0.7 to 2.6 V. c) Long-term cycling performance of the NaMnHCF//$NaTiOPO_4$ full battery. The current rate for the full battery is 0.2 C at the first eight cycles and then becomes 1C in the following cycles. d) The electrochemical parameters including average voltage, capacity based on the total mass of electrodes, energy density, and cycle life for various aqueous Na-ion batteries.

In summary, we developed a new class of IC-WiS electrolytes for ANIBs by introducing the tetraethylammonium triflate (TEAOTF) salt, which has a total concentration of 31 mol kg^{-1} (9 mol kg^{-1} NaOTF + 22 mol kg^{-1} TEAOTF) and a wide voltage window of 3.3 V. The large TEA^+ cations demonstrates inertness toward intercalation in both NaMnHCF cathode and $NaTiOPO_4$ anode, thus avoiding the cation cointercalation issue present in other mixed cation electrolytes. Moreover, the Na IC-WiS electrolyte reduces the dissolution of transition metal from the NaMnHCF cathode, markedly improving the cycling performance. The NaMnHCF//IC-WiS//$NaTiOPO_4$ full battery exhibits the highest average voltage (1.74 V) and energy density (71 Wh kg^{-1}) among other reported Na-based electrochemical couples, along with superior cycle stability at both low (90% retention after 200 cycles) and high (76% retention over 800 cycles) rates. The Na IC-WiS electrolyte opens up a new route to overcome the limitations associated with the sodium salt solubility and obtain superhigh concentration electrolyte, which not only promotes further advances for ANIBs, but also provides new design approaches for high-voltage aqueous batteries based on other (Li, K, Zn, and Al) systems.

Experimental Section

Materials Synthesis: The NaMnHCF cathode was prepared by a simple precipitation method. Typically, 2 mmol $Na_4Fe(CN)_6{\cdot}10H_2O$ and corresponding proportion of $MnSO_4{\cdot}H_2O$ were dissolved into 100 and 80 mL saturated NaCl solution, respectively. Then, these two solutions were slowly dropped together with magnetic stirring at 60 °C. After 12 h, the precipitate formed was centrifuged and washed thoroughly with deionized water. At last, the final product was obtained after drying in air under 80 °C for 12 h. The $NaTiOPO_4$ anode was synthesized by a simple hydrothermal reaction and ion-exchange process according to the previous literature.[39] The NaOTF salt (99%) was purchased from the TCI, and the TEAOTF salt (99%) was purchased from Shanghai Fujie Chemical Co., Ltd.

Electrochemical Measurements: To measure the ionic conductivities of the electrolytes, Pt electrode equipment with a specific conductivity constant are purchased from Shanghai Russell Technology Co., Ltd. The conductivity constant should be predetermined using 1 M aqueous KCl standard solution at 25 °C. Then, the ionic conductivities of the electrolytes can be obtained by measured electrochemical impedance spectroscopy (EIS) using electrochemical workstation (IM6e Zahner) in the oven at set temperature. Composite cathode (anode) electrodes were fabricated by compressing active materials, carbon black (super P), and poly(tetrafluorothylene) (PTFE) at weight ratio of 7:2:1 (6:3:1). The three-electrode cell for the cathode (anode) consists of NaMnHCF ($NaTiOPO_4$) composite as the working, AC as the counter and Ag/AgCl as the reference electrode, respectively. The full cell was assembled in pint-sized pouch cell using NaMnHCF cathode, $NaTiOPO_4$ anode and glass fiber as separator. The mass ratio of NaMnHCF/$NaTiOPO_4$ is 1/1.97 (1C = 0.14 A g^{-1}). The (9 molkg^{-1} NaOTF) means that 9 mmol NaOTF was dissolved in 1 mg water. The (9 molkg^{-1} NaOTF + 22 molkg^{-1} TEAOTF) represents 9 mmol NaOTF and 22 mmol TEAOTF were dissolved in 1 mg water. The ionic conductivity was measured with electrochemical impedance spectroscopy (EIS) with Gamry impedance analyzer.

Material Characterization: The structure was characterized using an X'Pert Pro MPD X-ray diffractometer (XRD) (D8 Bruker) with Cu Kα radiation (λ = 1.5405 Å) in the scan range (2θ) of 10°–80°. The morphologies of the cathodes were investigated by scanning electron microscopy (SEM, Hitachi-S4800). The TEM image of cycled $NaTiOPO_4$ anode is examined at a JEOL 2100 F field emission. The dissolving amount of the transition metal ions during cycling and specific ratios of Na, Fe, and Mn in the Cathodes were measured by inductively coupled plasma atomic emission spectrometry (ICP-AES). The water content of samples was estimated by thermogravimetric analysis (TGA). Linear sweep voltammetry was carried out using CHI 660E electrochemical work station. X-ray photoelectron spectra (XPS) were recorded with a spectrometer having Mg/Al Kα radiation (ESCALAB 250 Xi, ThermoFisher). All binding energies reported were corrected using the signal of carbon at 284.8 eV as an internal standard. The ^{17}O, ^{1}H, and ^{23}Na NMR spectra were acquired on a Bruker DRX 500 spectrometer. All NMR measurements were conducted at 303.2 K. The Raman spectra for electrolytes were collected with an NRS-5100 spectrometer (JASCO) using a 532 nm diode-pumped solid-state laser between 4000 and 100 cm^{-1}. Each electrolyte solution was placed in a quartz cell, and the laser was directed through the quartz crystal window.

MD Simulations: A periodic simulation cell comprised of 124 NaOTF, 304 TEAOTF, and 768 H_2O molecules yielding a linear dimension of 54.09 Å at 30 °C. A many-body polarizable force field APPLE&P was used.[49,50]

Supporting Information

Supporting Information is available from the Wiley Online Library or from the author.

Acknowledgements

This work was supported by National Key Technologies R&D Program, China (2016YFB0901500), the National Natural Science Foundation of China (51672275, 51421002, 51872322, and 51725206), the Strategic Priority Research Program of the Chinese Academy of Sciences (XDA21070500), and Beijing Municipal Science and Technology Commission (Z181100004718008). L.S. acknowledges the One Hundred Talent Project of the Chinese Academy of Sciences and Thousand Talents Program for Young Scientists. The Work at ARL was supported as part of the Joint Center for Energy Storage Research, an Energy Innovation Hub funded by the U.S. Department of Energy, Office of Science, Basic Energy Sciences through IAA SN2020957.

Conflict of Interest

The authors declare no conflict of interest.

Keywords

aqueous Na-ion batteries, inert cations, water-in-salt electrolytes

Received: July 10, 2019
Revised: October 24, 2019
Published online:

[1] Z. Yang, J. Zhang, M. C. Kintner-Meyer, X. Lu, D. Choi, J. P. Lemmon, J. Liu, *Chem. Rev.* **2011**, *111*, 3577.
[2] B. Dunn, H. Kamath, J.-M. Tarascon, *Science* **2011**, *334*, 928.
[3] H. Kim, J. Hong, K. Y. Park, H. Kim, S. W. Kim, K. Kang, *Chem. Rev.* **2014**, *114*, 11788.
[4] J. Y. Luo, W. J. Cui, P. He, Y. Y. Xia, *Nat. Chem.* **2010**, *2*, 760.
[5] H. Pan, Y. Shao, P. Yan, Y. Cheng, K. S. Han, Z. Nie, C. Wang, J. Yang, X. Li, P. Bhattacharya, K. T. Mueller, J. Liu, *Nat. Energy* **2016**, *1*, 16039.
[6] L. M. Suo, O. Borodin, T. Gao, M. Olguin, J. Ho, X. L. Fan, C. Luo, C. S. Wang, K. Xu, *Science* **2015**, *350*, 938.
[7] L. Suo, O. Borodin, Y. Wang, X. Rong, W. Sun, X. Fan, S. Xu, M. A. Schroeder, A. V. Cresce, F. Wang, C. Yang, Y.-S. Hu, K. Xu, C. Wang, *Adv. Energy Mater.* **2017**, *7*, 1701189.
[8] L. Suo, O. Borodin, W. Sun, X. Fan, C. Yang, F. Wang, T. Gao, Z. Ma, M. Schroeder, A. von Cresce, S. M. Russell, M. Armand, A. Angell, K. Xu, C. Wang, *Angew. Chem., Int. Ed.* **2016**, *55*, 7136.
[9] F. Wang, X. Fan, T. Gao, W. Sun, Z. Ma, C. Yang, F. Han, K. Xu, C. Wang, *ACS Cent. Sci.* **2017**, *3*, 1121.
[10] K. Nakamoto, R. Sakamoto, Y. Sawada, M. Ito, S. Okada, *Small Methods* **2018**, *3*, 1800220.
[11] J. Zhao, Y. Li, X. Peng, S. Dong, J. Ma, G. Cui, L. Chen, *Electrochem. Commun.* **2016**, *69*, 6.
[12] L. Jiang, Y. Lu, C. Zhao, L. Liu, J. Zhang, Q. Zhang, X. Shen, J. Zhao, X. Yu, H. Li, X. Huang, L. Chen, Y.-S. Hu, *Nat. Energy* **2019**, *4*, 495.
[13] Y. Yamada, K. Usui, K. Sodeyama, S. Ko, Y. Tateyama, A. Yamada, *Nat. Energy* **2016**, *1*, 16129.
[14] L. Suo, F. Han, X. Fan, H. Liu, K. Xu, C. Wang, *J. Mater. Chem. A* **2016**, *4*, 6639.
[15] F. Wang, O. Borodin, T. Gao, X. Fan, W. Sun, F. Han, A. Faraone, J. A. Dura, K. Xu, C. Wang, *Nat. Mater.* **2018**, *17*, 543.
[16] G. Hasegawa, K. Kanamori, T. Kiyomura, H. Kurata, T. Abe, K. Nakanishi, *Chem. Mater.* **2016**, *28*, 3944.
[17] Z. Tian, W. Deng, X. Wang, C. Liu, C. Li, J. Chen, M. Xue, R. Li, F. Pan, *Funct. Mater. Lett.* **2017**, *10*, 1750081.

[18] L. Xue, H. Gao, Y. Li, J. B. Goodenough, *J. Am. Chem. Soc.* **2018**, *140*, 3292.
[19] A. Zhou, Z. Xu, H. Gao, L. Xue, J. Li, J. B. Goodenough, *Small* **2019**, *15*, 1902420.
[20] L. Liu, X. Qi, S. Yin, Q. Zhang, X. Liu, L. Suo, H. Li, L. Chen, Y.-S. Hu, *ACS Energy Lett.* **2019**, *4*, 1650.
[21] L. Suo, D. Oh, Y. Lin, Z. Zhuo, O. Borodin, T. Gao, F. Wang, A. Kushima, Z. Wang, H. C. Kim, Y. Qi, W. Yang, F. Pan, J. Li, K. Xu, C. Wang, *J. Am. Chem. Soc.* **2017**, *139*, 18670.
[22] H. Zhang, S. Jeong, B. S. Qin, D. V. Carvalho, D. Buchholz, S. Passerini, *ChemSusChem* **2018**, *11*, 1382.
[23] M. H. Lee, S. J. Kim, D. Chang, J. Kim, S. Moon, K. Oh, K.-Y. Park, W. M. Seong, H. Park, G. Kwon, B. Lee, K. Kang, *Mater. Today*, **2019**, *29*, 26.
[24] M. R. Lukatskaya, J. I. Feldblyum, D. G. Mackanic, F. Lissel, D. L. Michels, Y. Cui, Z. Bao, *Energy Environ. Sci.* **2018**, *11*, 2876.
[25] V. V. Shcherbakov, *Russ. J. Electrochem.* **2009**, *45*, 1292.
[26] Y. Q. Yang, Z. Chang, M. X. Li, X. W. Wang, Y. P. Wu, *Solid State Ionics* **2015**, *269*, 1.
[27] D. Kumar, S. A. Hashmi, *Solid State Ionics* **2010**, *181*, 416.
[28] L. O. Valoen, J. N. Reimers, *J. Electrochem. Soc.* **2005**, *152*, A882.
[29] O. Borodin, L. Suo, M. Gobet, X. Ren, F. Wang, A. Faraone, J. Peng, M. Olguin, M. Schroeder, M. S. Ding, E. Gobrogge, A. von Wald Cresce, S. Munoz, J. A. Dura, S. Greenbaum, C. Wang, K. Xu, *ACS Nano* **2017**, *11*, 10462.
[30] J. X. Zheng, G. Y. Tan, P. Shan, T. C. Liu, J. T. Hu, Y. C. Feng, L. Y. Yang, M. J. Zhang, Z. H. Chen, Y. Lin, J. Lu, J. C. Neuefeind, Y. Ren, K. Amine, L. W. Wang, K. Xu, F. Pan, *Chem* **2018**, *4*, 2872.
[31] O. Borodin, G. A. Giffin, A. Moretti, J. B. Haskins, J. W. Lawson, W. A. Henderson, S. Passerini, *J. Phys. Chem. C* **2018**, *122*, 20108.
[32] O. Borodin, G. D. Smith, *J. Phys. Chem. B* **2006**, *110*, 4971.
[33] W. Huang, R. Frech, R. A. Wheeler, *J. Phys. Chem.* **1994**, *98*, 100.
[34] R. Frech, W. W. Huang, *J. Solution Chem.* **1994**, *23*, 469.
[35] X. Wu, Y. Qi, J. J. Hong, Z. Li, A. S. Hernandez, X. Ji, *Angew. Chem., Int. Ed.* **2017**, *56*, 13026.
[36] X. Wu, M. Shao, C. Wu, J. Qian, Y. Cao, X. Ai, H. Yang, *ACS Appl. Mater. Interfaces* **2016**, *8*, 23706.
[37] H. Ohtaki, T. Radnai, *Chem. Rev.* **1993**, *93*, 1157.
[38] H. Peng, A. V. Nguyen, *J. Mol. Liq.* **2018**, *263*, 109.
[39] L. Mu, L. Ben, Y.-S. Hu, H. Li, L. Chen, X. Huang, *J. Mater. Chem. A* **2016**, *4*, 7141.
[40] K. Nakamoto, R. Sakamoto, M. Ito, A. Kitajou, S. Okada, *Electrochemistry* **2017**, *85*, 179.
[41] C. Y. Liu, X. S. Wang, W. J. Deng, C. Li, J. T. Chen, M. Q. Xue, R. Li, F. Pan, *Angew. Chem., Int. Ed.* **2018**, *57*, 7046.
[42] L. Chen, H. Shao, X. Zhou, G. Liu, J. Jiang, Z. Liu, *Nat. Commun.* **2016**, *7*, 11982.
[43] X. Y. Wu, M. Y. Sun, Y. F. Shen, J. F. Qian, Y. L. Cao, X. P. Ai, H. X. Yang, *ChemSusChem* **2014**, *7*, 407.
[44] X. Wu, M. Sun, S. Guo, J. Qian, Y. Liu, Y. Cao, X. Ai, H. Yang, *ChemNanoMat* **2015**, *1*, 188.
[45] Z. Hou, X. Li, J. Liang, Y. Zhu, Y. Qian, *J. Mater. Chem. A* **2015**, *3*, 1400.
[46] Z. Li, D. Young, K. Xiang, W. C. Carter, Y.-M. Chiang, *Adv. Energy Mater.* **2013**, *3*, 290.
[47] H. Gao, J. B. Goodenough, *Angew. Chem., Int. Ed.* **2016**, *55*, 12768.
[48] A. J. Fernández-Ropero, D. Saurel, B. Acebedo, T. Rojo, M. Casas-Cabanas, *J. Power Sources* **2015**, *291*, 40.
[49] O. N. Starovoytov, O. Borodin, D. Bedrov, G. D. Smith, *J. Chem. Theory Comput.* **2011**, *7*, 1902.
[50] O. Borodin, *J. Phys. Chem. B* **2009**, *113*, 11463.

